Unraveling the structure and chemical mechanisms of highly oxygenated intermediates in oxidation of organic compounds

Zhandong Wang[a,1], Denisia M. Popolan-Vaida[b,c,d,e], Bingjie Chen[a], Kai Moshammer[f,g], Samah Y. Mohamed[a], Heng Wang[a], Salim Sioud[h], Misjudeen A. Raji[h], Katharina Kohse-Höinghaus[i], Nils Hansen[f], Philippe Dagaut[j], Stephen R. Leone[b,c,d], and S. Mani Sarathy[a,1]

[a]Clean Combustion Research Center, King Abdullah University of Science and Technology, Thuwal 23955-6900, Saudi Arabia; [b]Department of Chemistry, University of California, Berkeley, CA 94720; [c]Department of Physics, University of California, Berkeley, CA 94720; [d]Chemical Sciences Division, Lawrence Berkeley National Laboratory, Berkeley, CA 94720; [e]Department of Chemistry, University of Central Florida, Orlando, FL 32816-2450; [f]Combustion Research Facility, Sandia National Laboratories, Livermore, CA 94551; [g]Physikalisch-Technische Bundesanstalt, 38116 Braunschweig, Germany; [h]Analytical Core Laboratory, King Abdullah University of Science and Technology, Thuwal 23955-6900, Saudi Arabia; [i]Department of Chemistry, Bielefeld University, D-33615 Bielefeld, Germany; and [j]CNRS, Institut National des Sciences de l'Ingénierie et des Systèmes, Institut de Combustion, Aérothermique, Réactivité et Environnement, 45071, Orléans, Cedex 2, France

Edited by Donald G. Truhlar, University of Minnesota, Minneapolis, MN, and approved November 6, 2017 (received for review May 6, 2017)

Decades of research on the autooxidation of organic compounds have provided fundamental and practical insights into these processes; however, the structure of many key autooxidation intermediates and the reactions leading to their formation still remain unclear. This work provides additional experimental evidence that highly oxygenated intermediates with one or more hydroperoxy groups are prevalent in the autooxidation of various oxygenated (e.g., alcohol, aldehyde, keto compounds, ether, and ester) and nonoxygenated (e.g., normal alkane, branched alkane, and cycloalkane) organic compounds. These findings improve our understanding of autooxidation reaction mechanisms that are routinely used to predict fuel ignition and oxidative stability of liquid hydrocarbons, while also providing insights relevant to the formation mechanisms of tropospheric aerosol building blocks. The direct observation of highly oxygenated intermediates for the autooxidation of alkanes at 500–600 K builds upon prior observations made in atmospheric conditions for the autooxidation of terpenes and other unsaturated hydrocarbons; it shows that highly oxygenated intermediates are stable at conditions above room temperature. These results further reveal that highly oxygenated intermediates are not only accessible by chemical activation but also by thermal activation. Theoretical calculations on H-atom migration reactions are presented to rationalize the relationship between the organic compound's molecular structure (*n*-alkane, branched alkane, and cycloalkane) and its propensity to produce highly oxygenated intermediates via extensive autooxidation of hydroperoxyalkylperoxy radicals. Finally, detailed chemical kinetic simulations demonstrate the influence of these additional reaction pathways on the ignition of practical fuels.

autooxidation | peroxides | ignition | secondary organic aerosol | mass spectrometry

The autooxidation of volatile organic compounds (VOCs) influences the formation of tropospheric ozone (1) and secondary organic aerosols (SOAs) (2, 3), degradation of liquid and gaseous hydrocarbons (4, 5), as well as ignition processes in combustion (6). The chemistry of peroxy radical intermediates plays a significant role in autooxidation processes, because their H-shift and sequential O_2 addition reactions lead to the eventual formation of hydroperoxides, such as those found in liquid-phase hydrocarbon degradation (7, 8). Under atmospheric conditions (e.g., below 400 K), peroxy radical H-shift reactions compete with NO, HO_2, and peroxy radical biomolecular reactions that convert peroxy radicals to alkoxy radicals or closed-shell species such as nitrates, hydroperoxides, or carbonyls and alcohols, respectively (1, 9). Under low NO_x conditions, peroxy radical H-shift reactions provide a large source of low-volatility SOA in the atmospheric oxidation of monoterpenes (10, 11). At relatively higher temperatures (e.g., 500–800 K), the chemistry of peroxy radicals triggers interesting combustion phenomena such as cool flames (12) and negative temperature-coefficient behavior, leading to reactivity that decreases with increasing temperature (13), and to engine knock (14).

Existing kinetic models for gas-phase hydrocarbon combustion assume that one or two O_2 molecules add sequentially to the hydrocarbon radical, leading to intermediates with two or three O atoms on the hydrocarbon backbone (e.g., hydroperoxides, keto hydroperoxides, etc.), which ultimately dissociate to smaller species (15). However, recent work indicates that partially oxidized alkylperoxy radicals may undergo further sequential additions with O_2, thereby leading to more highly oxygenated intermediates (16, 17). Previous work on ozonolysis or OH-radical-initiated autooxidation of unsaturated hydrocarbons has identified the formation of highly oxygenated molecules from extensive autooxidation (EA) of peroxy radicals by abstraction of H atoms from C–H connected to

Significance

Highly oxygenated molecules are involved in autooxidation reactions leading to the formation of secondary organic aerosols (SOAs); they are also critical intermediates in autooxidation processes for liquid hydrogen degradation and the ignition of fuels in advanced combustion systems. However, these reactions are still poorly understood. In this study, we unveil a generalized reaction mechanism involving the autooxidation of peroxy radicals with at least three stages of sequential O_2 addition. We elucidate important underlying kinetics and structural characteristics of autooxidation processes used for developing new technologies including those aimed at reducing climatically active SOAs and pollutants from fuel combustion. We show that advances can be made by bridging experimental and theoretical methods used by atmospheric and combustion scientists.

Author contributions: Z.W., N.H., P.D., and S.M.S. designed research; Z.W., D.M.P.-V., B.C., K.M., S.Y.M., H.W., S.S., M.A.R., N.H., P.D., and S.M.S. performed research; Z.W. analyzed data; and Z.W., D.M.P.-V., K.K.-H., N.H., P.D., S.R.L., and S.M.S. wrote the paper.

The authors declare no conflict of interest.

This article is a PNAS Direct Submission.

[1]To whom correspondence may be addressed. Email: zhandong.wang@kaust.edu.sa or Mani.Sarathy@kaust.edu.sa.

This article contains supporting information online at www.pnas.org/lookup/suppl/doi:10.1073/pnas.1707564114/-/DCSupplemental.

oxygenated functional groups (OH and C=O), allylic sites, and other weakly bound H atoms (10, 18–21). Under atmospheric conditions, Jokinen et al. (22) stated that intramolecular H-shift reactions are important only if relatively weak C–H bonds are available. Crounse et al. (23) also showed that functionalized species with carbonyl, alcohol, or alkene moieties are needed to facilitate H-shift reactions at room temperature.

Here, we detect highly oxygenated intermediates involved in the autooxidation of alkanes at 500–600 K. This temperature range and class of hydrocarbons are rarely investigated in atmospheric studies. We build on experimental and theoretical advances in atmospheric autooxidation chemistry research to study related processes under combustion conditions. Isotopic labeling methods demonstrated in atmospheric studies (10, 18–20) are combined with photoionization and high-resolution mass spectrometry methods in combustion research (24) to unravel the complex structure of autooxidation intermediates. We show the presence of at least three O_2 molecules adding sequentially to hydrocarbon/oxygenated radicals during gas-phase oxidation in the temperature range 500–600 K; the oxygen-containing functional groups in the highly oxygenated intermediates are also identified. These findings complement previous atmospheric autooxidation chemistry research, while extending our understanding of autooxidation processes and the prevailing reaction mechanisms used to numerically simulate fuel autoignition.

The gas-phase autooxidation of 15 VOCs was systematically examined to study the key autooxidation intermediates. Ten compounds were drawn from the four major hydrocarbon classes (i.e., normal, branched, and cyclo alkanes and aromatics); an additional five compounds have oxygen-containing functional groups (25) (1-decanol, decanal, 2-decanone, dipentyl ether, and methyl decanoate). The species were selected to represent VOCs present in tropospheric and fuel/engine oxidation environments. Autooxidation studies were carried out in two separate fused-silica jet-stirred reactors (JSR), operating at a mean residence time of 2 s, near atmospheric pressure and temperatures from 500 to 600 K. JSR-1 was coupled to a molecular beam time-of-flight mass spectrometer (MBMS), combined with synchrotron vacuum UV (SVUV) radiation from a third-generation synchrotron source as the photoionization (PI) source (26, 27). The gas-phase products from JSR-2 were analyzed by a high-resolution atmospheric pressure chemical ionization-Orbitrap mass spectrometer (APCI-OTMS) (28–30) (*SI Appendix*, section 1.1, Fig. S1, and Table S1).

Results and Discussion

Many autooxidation intermediates were measured from the autooxidation of the 15 VOCs (i.e., $C_xH_yO_z$) in the SVUV-PI-MBMS and APCI-OTMS experiments. Autooxidation products, with the general molecular formula $C_xH_{y-2}O_{z+n}$ ($n = 0$–5) and $C_xH_{y-4}O_{z+n}$ ($n = 4$), were consistently observed, with only a few exceptions for $C_xH_{y-2}O_{z+n}$ ($n = 4$) due to low signal intensity (*SI Appendix*, Figs. S2–S8). Here, x equals the carbon number of the organic compounds; y is equal to $2x + 2$ for alkanes, alcohols, and ethers, $2x$ for cycloalkanes, aldehydes, ketone compounds, and esters; z is equal to 0 for hydrocarbons, 1 for alcohols, aldehydes, ketone compounds, and ethers, and 2 for esters. A glossary of species discussed in the text is provided in *SI Appendix*, section 1.3. Fig. 1 shows a generalized peroxy radical oxidation mechanism comprising sequential oxygen addition and radical isomerization reactions that lead to the formation of various intermediates. The specific mechanism diagrams of 2,7-dimethyloctane and *n*-butylcyclohexane are shown in *SI Appendix*, section 1.4 and Schemes S1 and S2. The intermediates $C_xH_{y-2}O_{z+n}$ ($n = 0$–1) and $C_xH_{y-2}O_{z+n}$ ($n = 2$–3) derive from the first and second oxygen addition reactions, a reaction mechanism established in the 1980s (6) and widely adopted in combustion modeling (15). $C_xH_{y-2}O_{z+n}$ ($n = 4$–5) intermediates are the result of third

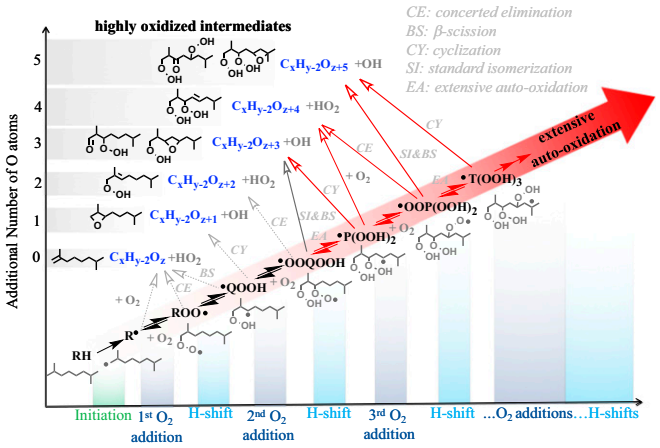

Fig. 1. Generalized autooxidation mechanism of organic compounds (i.e., $C_xH_yO_z$), involving formation of intermediates with molecular formula of $C_xH_{y-2}O_{z+n}$ (n = 0–5, labeled in blue and boxed). The structures of probable intermediates for autooxidation of R with a radical site at the primary carbon of 2,7-dimethyloctane are presented. Pathways to $C_xH_{y-2}O_5$ and $C_xH_{y-2}O_3$ highly oxygenated intermediates are highlighted with bold arrows. The extensive autooxidation and third sequential oxygen addition reaction pathways are denoted by red arrows. Intramolecular H-atom abstraction of the C–H alpha to the -OOH group by an –OO is a standard isomerization; intramolecular H-atom abstraction from a C–H not alpha to the –OOH group by an –OO is an extensive autooxidation.

oxygen addition reactions, and these reaction pathways are labeled in red in Fig. 1. $C_xH_{y-2}O_{z+n}$ ($n = 3$) are also formed from these reactions, but the resulting structures are different from those formed from the second oxygen addition reactions. Details of the reaction mechanism will be described after discussing the elemental composition and structure of the measured intermediates. At 500–600 K, peroxy radical isomerization reactions compete with bimolecular reactions (e.g., cross-combination and recombination of RO_2) and formation of dimer compounds (1, 18). For example, the rate constant of $RO_2 + RO_2$ (e.g., $C_2H_5O_2 + C_2H_5O_2$) is on the order of 10^{10} $cm^3 \cdot mol^{-1} \cdot s^{-1}$ at 298 K and has a weak negative temperature dependence (31), while the intramolecular H-atom abstraction of the RO_2 radical via a six-membered-ring transition state is on the order of 10^{-3} s^{-1} at 298 K (23). However, the intramolecular H-atom abstraction is strongly temperature dependent and its rate is on the order of 10^4 s^{-1} at 550 K (32). This is one feature of alkane autooxidation in the low-temperature combustion environment that is distinct from ozonolysis and/or OH-radical-initiated autooxidation of unsaturated hydrocarbons in which dimer compounds were observed to be important (10, 18, 19).

Elemental C/H/O Composition of Highly Oxygenated Intermediates. Initially, the elemental C/H/O composition of highly oxygenated intermediates was confirmed to have the same carbon number as the VOC reactant with three to five additional oxygen atoms. To enhance molecular information within the instrument's mass resolution, unambiguous elemental composition was obtained via isotope labeling, using both $^{16}O_2$ and then $^{18}O_2$ as the oxidizers in autooxidation of 2,7-dimethyloctane and cyclohexane. Fig. 2*A* for 2,7-dimethyloctane ($C_{10}H_{22}$) shows that replacing $^{16}O_2$ by $^{18}O_2$ increases the mass-to-charge ratio, m/z, of highly oxygenated intermediates $C_{10}H_{20}O_3$, $C_{10}H_{18}O_4$, $C_{10}H_{20}O_4$, and $C_{10}H_{20}O_5$ by 6, 8, 8, and 10, respectively. Similarly, species featuring 3, 4, or 5 oxygen atoms were identified in the case of cyclohexane autooxidation using isotopically labeled O_2 (*SI Appendix*, Fig. S9). The formation of highly oxygenated intermediates was further corroborated for both VOCs by the high-resolution APCI-OTMS experiment, which observed the protonated molecular

CHEMISTRY

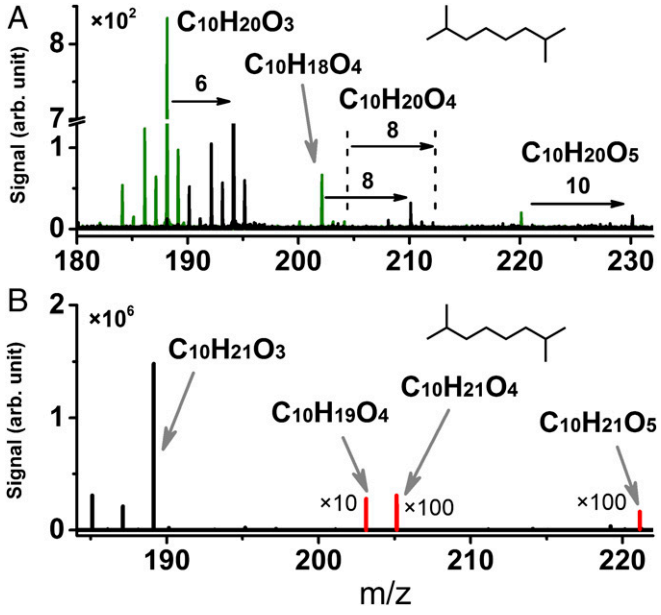

Fig. 2. Mass spectra of highly oxygenated intermediates recorded in 2,7-dimethyloctane autooxidation. (*A*) SVUV-PI-MBMS results at photon energy of 9.5 eV with $^{16}O_2$ (green line) and $^{18}O_2$ (black line) as the oxidizer. (*B*) APCI-OTMS results with $^{16}O_2$ as oxidizer. Protonated molecular ion peaks $C_{10}H_{18}O_4$, $C_{10}H_{20}O_4$, and $C_{10}H_{20}O_5$ multiplied by 10, 100, and 100, respectively, for clarity.

peaks of $C_{10}H_{20}O_3$, $C_{10}H_{18}O_4$, $C_{10}H_{20}O_4$, and $C_{10}H_{20}O_5$ (accuracy < 5 ppm, Fig. 2*B*) for 2,7-dimethyloctane and analogous highly oxygenated intermediates for cyclohexane (*SI Appendix*, Fig. S9). Similar oxygenated hydrocarbon species have been detected from the atmospheric ozonolysis and autooxidation of monoterpenes and their surrogates under low concentration of NO_x (10, 11, 18), which establishes the relevance of the present findings with atmospheric chemical processes.

H/D Exchange Reactions. The signal profiles for $C_{10}H_{20}O_3$, $C_{10}H_{18}O_4$, $C_{10}H_{20}O_4$, and $C_{10}H_{20}O_5$ from 2,7-dimethyloctane are typical of hydroperoxides formed during hydrocarbon oxidation (*SI Appendix*, Fig. S10); they are produced in early stages of oxidation and consumed rapidly at higher temperatures because of the low O–OH bond dissociation energy in the hydroperoxy group (8). Hydroperoxides are important in controlling hydrocarbon reactivity during autooxidation (15, 33).

The presence of hydroperoxy functional groups was confirmed by H/D exchange reactions using D_2O in JSR-1 coupled with SVUV-PI-MBMS. H/D exchange reactions have been used in the field of atmospheric chemistry to identify -OH/-OOH functional groups (10, 18–20). However, it was unclear if H atoms in other functional groups could participate in exchange reactions with D_2O at higher temperature (e.g., 500–600 K). Therefore, we confirmed that only H atoms in –OH and –OOH functional groups (i.e., acidic H atoms) participate in H/D exchange reactions for the selected conditions by reacting D_2O with 2,7-dimethyloctane, as well as ethanol, propanal, acetone, tetrahydrofuran, methyl peroxide, and hydrogen peroxide (*SI Appendix*, section 1.7 and Fig. S11). Products resulting from the autooxidation of 2,7-dimethyloctane with D_2O further supported the finding that only acidic H atoms participated in H/D exchange reactions. The mass spectra obtained for 2,7-dimethyloctane autooxidation in Fig. 3 *A–C* show the signal intensities for $C_{10}H_{20}O_3$, $C_{10}H_{18}O_4$, and $C_{10}H_{20}O_5$, with and without the addition of ~50,000 ppm D_2O to the reactants. A clear indication for H/D exchange upon D_2O addition is seen from the decreasing signal intensity of $C_{10}H_{20}O_3$, $C_{10}H_{18}O_4$, and $C_{10}H_{20}O_5$, and appearance of $C_{10}H_{19}DO_3$, $C_{10}H_{17}DO_4$, $C_{10}H_{19}DO_5$, and $C_{10}H_{18}D_2O_5$. We note that a weak signal near *m/z* 190 is the isotopic peak of $C_{10}H_{19}DO_3$. Further evidence is provided in Fig. 3 *D–F*, which shows the photoionization efficiency spectra of $C_{10}H_{20}O_3$, $C_{10}H_{18}O_4$, and $C_{10}H_{20}O_5$ and the corresponding deuterated compounds, $C_{10}H_{19}DO_3$, $C_{10}H_{17}DO_4$, $C_{10}H_{19}DO_5$, and $C_{10}H_{18}D_2O_5$. Photoionization efficiency spectra were obtained by scanning photon energy, and the relationship between structure and photoionization behavior was used for species' identification (24, 34). The applicability of this methodology is limited for high-molecular-weight hydrocarbons due to the large number of possible isomers (34). Fig. 3 *D–F* shows that both hydrogenated and deuterated compounds contribute to the observed spectra, and their near-identical photoionization efficiency spectra indicate their identical structures. Current knowledge of hydrocarbon autooxidation mechanisms would suggest that bimolecular reactions of peroxy radicals, as well as bimolecular reactions of alkoxy radicals, lead to oxygenated intermediates with –OH functional groups (7, 35). However, these oxygenates do not correspond to the highly oxygenated intermediates observed in this work. Thus, the exchange experiments conclude that the detected intermediate $C_{10}H_{20}O_3$ contains one –OOH group, $C_{10}H_{18}O_4$ contains one –OOH group, and $C_{10}H_{20}O_5$ contains two –OOH groups. The H/D exchange reaction between $C_{10}H_{18}O_4$ and D_2O also produces $C_{10}H_{16}D_2O_4$ (a smaller peak than that of $C_{10}H_{17}DO_4$), as shown in Fig. 3 *B* and *E*. These results indicate that $C_{10}H_{18}O_4$ may contain isomers with two –OOH groups (e.g., dienes with two –OOH groups).

The presence of hydroperoxy functional groups in these oxygenates is further supported by both the nature and the similar temperature-dependent behavior of their fragments (*SI Appendix*, Fig. S10). The ions $C_{10}H_{19}O^+$ and $C_{10}H_{19}O_2^+$ (*SI Appendix*, Fig. S10*A*) are plausible fragments of the primary ion $C_{10}H_{20}O_3^+$, after elimination of –OOH and through dissociation of the O–OH bond in the hydroperoxy group, respectively. Similarly, $C_{10}H_{17}O_2^+$ and $C_{10}H_{19}O_3^+$ (*SI Appendix*, Fig. S10 *B* and *D*) are likely the

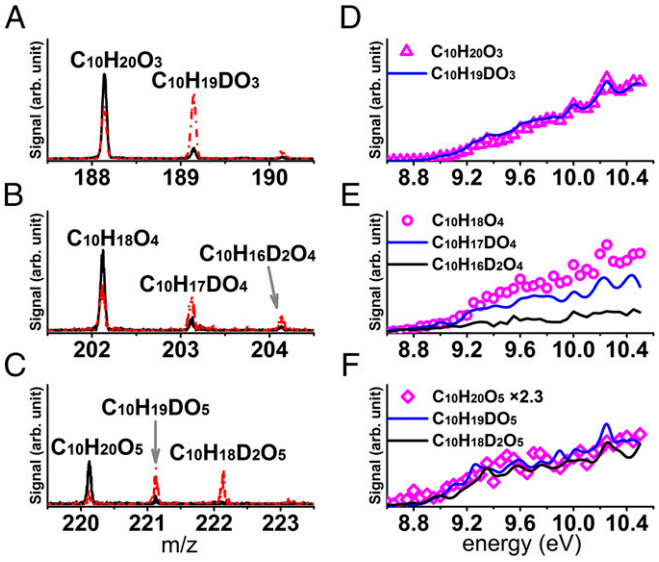

Fig. 3. Photoionization mass spectra and photoionization efficiency spectra of $C_{10}H_{20}O_3$, $C_{10}H_{18}O_4$, and $C_{10}H_{20}O_5$ with and without D_2O addition. (*A–C*) Mass spectra of $C_{10}H_{20}O_3$, $C_{10}H_{18}O_4$, and $C_{10}H_{20}O_5$ with (dashed red line) and without D_2O addition (black line) at 530 K and 9.5 eV. (*D–F*) Photoionization efficiency spectra of $C_{10}H_{20}O_3$, $C_{10}H_{18}O_4$, and $C_{10}H_{20}O_5$ (open symbols) and their corresponding deuterated species (lines) at 530 K. Signal of $C_{10}H_{20}O_5$ in *F* multiplied by 2.3.

products of the primary ions $C_{10}H_{18}O_4^+$ and $C_{10}H_{20}O_5^+$ after elimination of –OOH.

Autooxidation Mechanism Involving Sequential Oxygen Addition. Similar distributions of autooxidation intermediates (*SI Appendix*, Figs. S2–S8) and their fragments (*SI Appendix*, Table S2) were observed during oxidation of the other 12 VOCs in the SVUV-PI-MBMS experiment. This information on autooxidation intermediates motivates us to establish a general mechanistic understanding of their formation and destruction. Specifically, the reactions involving the first, second, and third sequential O_2 addition steps are addressed in the oxidation of VOCs with the general formula $C_xH_yO_z$ [i.e., reactions involved in the formation of autooxidation intermediates with the general formula $C_xH_{y-2}O_{z+n}$ (n = 0–5)]. Fig. 1 illustrates a generalized reaction mechanism and the pertinent processes for 2,7-dimethyloctane autooxidation.

First and second oxygen addition. The reaction sequence starts with H-atom abstraction from the parent organic molecule (i.e., $C_xH_yO_z$, $C_{10}H_{22}$) to produce a radical R ($C_xH_{y-1}O_z$, $C_{10}H_{21}$). Italicized text within parentheses denotes intermediate species in 2,7-dimethyloctane oxidation. H-atom abstraction occurs at primary, secondary, and tertiary carbon sites of 2,7-dimethyloctane. Fig. 1 shows the structure of the probable intermediates from the autooxidation of R with the radical site at the primary carbon. Intramolecular H-atom abstraction of ROO, OOQOOH, and $OO(POOH)_2$ radicals, via a six-membered-ring transition state (TS), is considered. Three sequential steps of O_2 addition (solid arrows in Fig. 1) lead to highly oxygenated intermediates [i.e., $C_xH_{y-2}O_{z+n}$ (n = 3–5), $C_{10}H_{20}O_3$, $C_{10}H_{20}O_4$, and $C_{10}H_{20}O_5$]. The first O_2 addition to the radical R produces an alkylperoxy radical (ROO, $C_{10}H_{21}OO$) that may isomerize to a hydroperoxyalkyl radical (36) (QOOH, $C_{10}H_{20}OOH$). A second O_2 addition to QOOH yields a hydroperoxyalkylperoxy radical (OOQOOH, $OOC_{10}H_{20}OOH$). Intramolecular H-atom abstraction of the C–H alpha to the -OOH group in OOQOOH, with subsequent β-O-O scission, forms highly oxygenated intermediates $C_xH_{y-2}O_{z+3}$ (with one C=O and one -OOH) and one OH radical. Here, the intramolecular H-atom abstraction of the C–H alpha to the -OOH group by an –OO via five- to eight-membered TS is defined as the standard isomerization, while intramolecular H-atom abstraction by an –OO via five- to eight-membered-ring TS from a C–H not alpha to the –OOH is the EA. The competition between standard isomerization and EA is determined by the TS ring size and the carbon type being abstracted (32). A few of these postulated reaction intermediates and their plausible structures have been recently identified in the low-temperature oxidation of selected VOC compounds, including *n*-butane (24, 33), *n*-pentane (37), 2-methylhexane (17), and dimethyl ether (26). An EA pathway leads to a radical $P(OOH)_2$, which can undergo cyclization to produce OH radical and a species of formula $C_xH_{y-2}O_{z+3}$, albeit with one O heterocycle and one –OOH functional group.

Third oxygen addition. The abundance of isomers for highly oxygenated intermediates and the numerous possible structures and conformers have historically made it difficult to follow the autooxidation mechanism, even for two sequential oxygen additions (17, 26). However, this study makes it possible to follow these reactions for a third sequential O_2 addition in which O_2 adds to the radical site of $P(OOH)_2$ [e.g., $C_{10}H_{19}(OOH)_2$] and produces an $OOP(OOH)_2$ radical [e.g., $OOC_{10}H_{19}(OOH)_2$]. The unambiguous results from the oxygen isotope labeling and the H/D exchange experiments indicate (for 15 representatives of prototypical VOC classes) that reaction sequences occur similarly to those for the OOQOOH radicals obtained after sequential addition of two O_2 molecules. The standard isomerization of $OOP(OOH)_2$ and subsequent β-O-O scission forms $C_xH_{y-2}O_{z+5}$ (with one C=O and two -OOHs, $C_{10}H_{20}O_5$) and OH radical; the EA of $OOP(OOH)_2$ leads to the $T(OOH)_3$ radical [e.g., $C_{10}H_{18}(OOH)_3$]. Further cyclization of $T(OOH)_3$ also produces $C_xH_{y-2}O_{z+5}$ (with one O heterocycle and two -OOHs, $C_{10}H_{20}O_5$) and one OH radical. The reaction of $P(OOH)_2$ with O_2, the concerted elimination of $OOP(OOH)_2$, and the β-C-O scission of $T(OOH)_3$ (not shown in Fig. 1) form $C_xH_{y-2}O_{z+4}$ (with one C=C and two -OOHs, $C_{10}H_{20}O_4$) and one HO_2 radical.

With the addition of three sequential oxygen molecules, additional reactions (denoted by dashed arrows in Fig. 1) may occur to form $C_xH_{y-2}O_z$ (with one C=C, $C_{10}H_{20}$), $C_xH_{y-2}O_{z+1}$ (with one O heterocycle, $C_{10}H_{20}O$), and $C_xH_{y-2}O_{z+2}$ (with one C=C and one -OOH, $C_{10}H_{20}O_2$). Note that the measured $C_xH_{y-2}O_{z+2}$ signal in this work may contain a contribution from secondary reactions, e.g., keto alcohols, from the bimolecular reactions of keto-alkoxy radicals (7).

Briefly, this reaction scheme explains the formation of the autooxidation intermediates: The highly oxygenated intermediates $C_xH_{y-2}O_{z+n}$ (n = 3–5) contain one or two hydroperoxy (-OOH) groups and other functional groups include carbonyl (C=O), cyclic ether (O heterocycle), and alkene (C=C). The $C_xH_{y-4}O_{z+4}$ (with one and/or two –OOHs, $C_{10}H_{18}O_4$) intermediates may be derived from subsequent reactions of $C_xH_{y-2}O_{z+5}$ (e.g., $C_{10}H_{20}O_5$), such as OH-radical-assisted water elimination (16, 35) and/or secondary reactions of $C_xH_{y-2}O_{z+2}$ (e.g., $C_{10}H_{20}O_2$). Their formation and relative ratios are not expected to significantly alter the overall radical pool. It could be assumed that $T(OOH)_3$ undergoes further O_2 addition and subsequent intramolecular H shift to form intermediates with even higher oxygen content, especially for organic compounds with longer carbon chains, appropriate functional groups, and in oxidation processes with adequate concentration of O_2 and appropriate temperature. Thus, the sequential addition of oxygen, as defined here, may not end after the third step.

Extensive Peroxy Radical Autooxidation. An interesting aspect of the proposed reaction mechanism is the EA of OOQOOH and subsequent third O_2 addition pathways. To provide further insights into this reaction type, Fig. 4 presents the relative ratios of $C_xH_{y-2}O_5$ to $C_xH_{y-2}O_3$ from autooxidation of *n*-heptane, 2-methylhexane (17), 2,5-dimethylhexane (16), cycloheptane, *n*-decane, 2-methylnonane, 2,7-dimethyloctane, and *n*-butylcyclohexane (*SI Appendix*, section 1.9 and Fig. S12). $C_xH_{y-2}O_5$ and $C_xH_{y-2}O_3$ are representative products from the third and second O_2 addition, respectively, as highlighted in Fig. 1. The ratio of these two intermediates indicates the likelihood of the EA isomerization of OOQOOH and third O_2 addition reaction and the propensity to produce higher oxygenated species (i.e., $C_xH_{y-2}O_5$). Note that the cyclization of $P(OOH)_2$ also forms $C_xH_{y-2}O_3$, but simulations have proven that $C_xH_{y-2}O_3$ is primarily formed via the standard isomerization of OOQOOH (17, 38). Fig. 4 shows that $C_xH_{y-2}O_5$'s yield depends on the molecular structure of the VOC. For example, *n*-heptane has the lowest yield, 2-methylhexane and 2,5-dimethylhexane have an intermediate yield, and cycloheptane has the highest yield among the C_7 and C_8 alkanes. An analogous tendency to form $C_xH_{y-2}O_5$ is observed for the C_{10} alkanes in the order of *n*-decane < 2-methylnonane < 2,7-dimethyloctane < *n*-butylcyclohexane, indicating that hydrocarbons with a tertiary C–H site and ring structures favor the formation of $C_xH_{y-2}O_5$ highly oxygenated intermediates.

EA is a prerequisite for the production of $C_xH_{y-2}O_5$ highly oxygenated intermediates. The tertiary C–H site and ring structures that favor the EA process permit intramolecular H-abstraction reactions to proceed via a six-membered-ring TS, since they are the most favorable pathways (15). Numerous OOQOOH radicals can be produced from the autooxidation process. Several typical α,γ-OOQOOHs, from normal alkane, branched alkane, and cycloalkane, have been chosen for discussion here. α is the position of the –OO group while γ is the position of the –OOH group. The activation energies and entropy changes for intramolecular

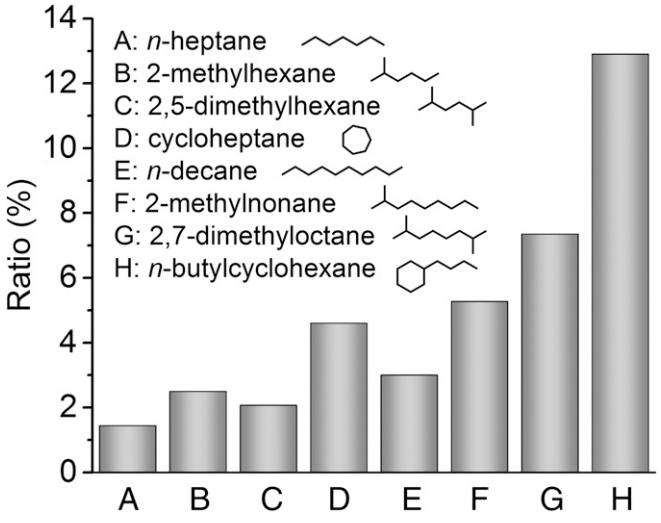

Fig. 4. Relative ratios of $C_xH_{y-2}O_5$ to $C_xH_{y-2}O_3$ in eight hydrocarbon autooxidation reactions (*A–H*), indicating the likelihood of extensive autooxidation of OOQOOH and third O_2 addition reaction, which affect the propensity to produce heavier highly oxygenated intermediates (i.e., $C_xH_{y-2}O_5$). Data for 2-methylhexane and 2,5-dimethylhexane autooxidation from Wang et al. (16, 17).

H-abstraction reactions in Fig. 5 *A–C* have been computed from quantum calculations. Details of the kinetic analysis with temperature are shown in *SI Appendix*, section 2.1 and Fig. S13. The peroxy radicals investigated in this work have a high degree of torsional anharmonicity, which can lead to discrepancies in partition function calculations (39, 40). Further study on the standard isomerization and EA of the peroxy radicals using more accurate treatment of the thermodynamic and kinetics calculations is needed.

The kinetic analysis reveals that EA of α,γ-OOQOOH radical A, B, and C in Fig. 5 is feasible. An EA of OOQOOH radical by abstracting a tertiary C-H is preferred over an EA by abstracting primary or secondary C–Hs; this is attributed to the lower activation energy and higher entropy difference to form the transition state in the former pathway. Moreover, the equilibrium constant of OOQOOH radical's EA by abstracting a tertiary C–H is higher than that of a secondary C–H (*SI Appendix*, Fig. S14). Thus, increasing the number of tertiary C–Hs from *n*-decane to 2-methylnonane and to 2,7-dimethyloctane, kinetically and thermodynamically, promotes the EA process. Furthermore, as shown in Fig. 5*D*, when the -OOH is on a tertiary carbon site, the α,γ-OOQOOH radical can undergo an EA isomerization to produce $C_xH_{y-2}O_5$ intermediates, while the pathway of standard isomerization to $C_xH_{y-2}O_3$ intermediates is impossible due to the lack of H-atoms alpha to the –OOH site.

For α,γ-OOQOOH generated from cycloalkanes, 2^n stereoisomers can be formed where "*n*" is the number of the chiral center. For instance, α,γ-OOQOOH (i.e., hydroperoxy-cyclohexyl peroxy) generated from cyclohexane has four stereoisomers, which are ax-OOH-ax-OO, ax-OOH-eq-OO, eq-OOH-ax-OO, and eq-OOH-eq-OO (ax: axial position, eq: equatorial position, *SI Appendix*, Fig. S15). There is only one isomer (eq-OOH-ax-OO) that can undergo the standard isomerization pathways, whereas the other three favor an EA of OOQOOH, leading to $C_xH_{y-2}O_5$ intermediates. Fig. 5*E* presents the ax-OOH-ax-OO, confirmed to be the most stable conformer due to the hydrogen bonding effect between the hydroperoxy and peroxy groups (*SI Appendix*, Fig. S15 and Table S3). The potential energy surface shows that the 1,5-hydrogen EA, which involves an abstraction of the axial-C–H (C5-H in Fig. 5*E*) via a six-membered-ring TS, has the lowest energy barrier (28.8 kcal/mol), resulting in a meta secondary $P(OOH)_2$ radical (*SI Appendix*, Fig. S16). The structure of the axial–axial conformer hinders the formation of $C_xH_{y-2}O_3$ (keto-hydroperoxide) because the standard isomerization process by intramolecular H abstraction of the equatorial-C–H alpha to the OOH group is impossible without altering the cyclic chair structure.

Cycloalkanes containing alkyl side chains further promote the production of $C_xH_{y-2}O_5$ intermediates, as in the case of *n*-butylcyclohexane. Fig. 5*F* shows one exemplary α,γ-OOQOOH radical in *n*-butylcyclohexane autooxidation, where the –OOH and –OO are both at the axial position and the *n*-butyl is at the equatorial position. The –OO group can abstract the axial C–H of carbon site five in the ring, or abstract the C–H of carbon site seven in the side chain via six-membered-ring TS. The free rotation of the side chain significantly reduces the energy barrier from 26.4 kcal/mol (41) to 21 kcal/mol (42), which then accelerates the EA process in *n*-butylcyclohexane.

Summary and Conclusions

In summary, highly oxygenated intermediates with one to two hydroperoxy groups were detected during the autooxidation of 15 organic compounds at combustion-relevant temperatures, and a peroxy radical reaction mechanism with three stages of sequential O_2 addition was confirmed. A combination of experimental techniques was used to determine the structures and functional groups of these elusive intermediate species. Experimental observations for different VOC structures, combined with a kinetics analysis, highlighted the role of EA isomerization reactions in forming highly oxygenated intermediates. Including these reaction pathways in chemical kinetic simulations was shown to decrease the ignition delay time predictions of *n*-heptane/O_2/N_2 mixtures at 600 K, with an ~20% reduction at 1 bar and 60% reduction at 50 bar (*SI Appendix*, Fig. S17 and Table S4).

O–OH bond dissociation in hydroperoxy groups of highly oxygenated intermediates plays an important role in radical chain branching that drives ignition processes in combustion engines. The $C_xH_{y-2}O_5$ intermediates produced via the third sequential O_2 addition scheme are additional radical chain-branching intermediates (16) which may extend ignition limits under certain conditions (43). The absence of these additional radical chain

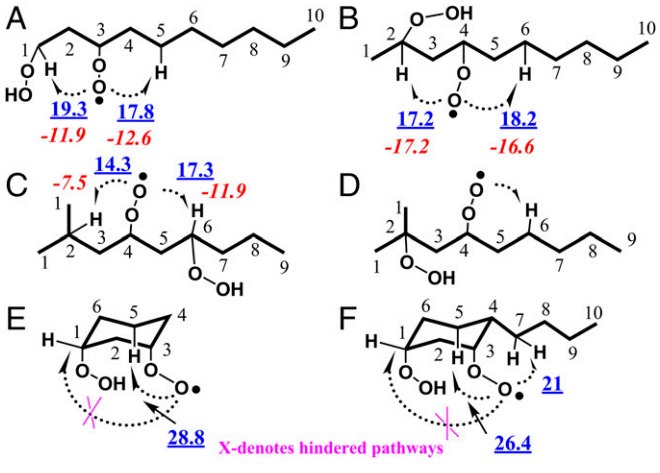

Fig. 5. Structural analysis of α,γ-OOQOOH intramolecular H abstraction. Blue underlined numbers denote activation energy, unit is kcal/mol; red italicized numbers denote entropy change, unit is cal/mol/K. Activation energies and entropy change of intramolecular H-abstraction reactions in *A–C* and activation energy in *E* were computed as described in *SI Appendix*, section 2. The activation energy and entropy change for the extensive autooxidation pathway in *D* is not shown since a competing standard isomerization pathway does not exist. Activation energies of 26.4 and 21 kcal/mol in *F* estimated from quantum-chemistry calculations of Xing et al. (41) and Ning et al. (42), respectively.

branching pathways in simulations may explain the underprediction of ignition delay time of long chain alkanes at high pressures (44). It is possible that intermediates with even higher oxygen content may be produced under low-temperature and high-pressure combustion conditions. This autooxidation mechanism also has implications for the formation of cool flames in alkane fuel droplets under microgravity conditions (45). This chemistry is important in liquid hydrocarbon degradation in the temperature range of 400–500 K (7), which is relevant to the oxidative stability of lubricants and other industrial fluids. The formation of atmospheric SOA under low NO_x concentrations (10) is also driven by similar chemical processes. The experimental results presented here for molecules with oxygen-containing functional groups (e.g., carbonyl and hydroxy) are in agreement with prior theoretical work on mechanisms for creating and aging the organic content of atmospheric particulate matter (23). Further advances in understanding autooxidation processes can be achieved by bridging experimental and theoretical methods used by atmospheric and combustion scientists.

ACKNOWLEDGMENTS. The authors thank Elisabeth Lutanie, Virginia Unkefer, and Ivan Gromicho (Research Publication Services, KAUST) for editorial assistance; Dr. Mikael Ehn and Dr. Matti P. Rissanen (University of Helsinki) and Dr. William H. Green (Massachusetts Institute of Technology) for valuable discussions; and Paul Fugazzi for technical support. This work was supported by King Abdullah University of Science and Technology, Office of Sponsored Research (OSR) under Award OSR-2016-CRG5-3022, and Saudi Aramco under the FUELCOM program (to Z.W., B.C., S.Y.M., H.W., and S.M.S.); Director, Office of Energy Research, Office of Basic Energy Sciences (BES), Chemical Sciences Division of the US Department of Energy (USDOE), Gas Phase Chemical Physics Program, under Contract DE-AC02-05CH11231 (to D.M.P.-V. and S.R.L.); Division of Chemical Sciences, Geosciences and Biosciences, BES/USDOE (N.H. and K.M.); Deutsche Forschungsgemeinschaft Project KO1363/31-1 (to K.K.-H.); European Research Council (ERC) under FP7/2007-2013/ERC Grant 291049-2G-CSafe (to P.D.). Sandia National Laboratories is a multimission laboratory managed and operated by National Technology and Engineering Solutions of Sandia, LLC, a wholly owned subsidiary of Honeywell International, Inc., for the USDOE's National Nuclear Security Administration under Contract DE-NA0003525. The Advanced Light Source is supported by the Director, Office of BES, of the USDOE under Contract DE-AC02-05CH11231.

1. Calvert JG, Derwent RG, Orlando JJ, Tyndall GS, Wallington TJ (2008) *Mechanisms of Atmospheric Oxidation of the Alkanes* (Oxford Univ Press, Oxford), pp 13–27.
2. Lim YB, Ziemann PJ (2005) Products and mechanism of secondary organic aerosol formation from reactions of *n*-alkanes with OH radicals in the presence of NO_x. *Environ Sci Technol* 39:9229–9236.
3. Claeys M, et al. (2004) Formation of secondary organic aerosols through photooxidation of isoprene. *Science* 303:1173–1176.
4. Ingold KU (1961) Inhibition of the autoxidation of organic substances in the liquid phase. *Chem Rev* 61:563–589.
5. Porter NA (1986) Mechanisms for the autoxidation of polyunsaturated lipids. *Acc Chem Res* 19:262–268.
6. Cox RA, Cole JA (1985) Chemical aspects of the autoignition of hydrocarbon-air mixtures. *Combust Flame* 60:109–123.
7. Jensen RK, Korcek S, Mahoney LR, Zinbo M (1979) Liquid-phase autoxidation of organic compounds at elevated temperatures. 1. The stirred flow reactor technique and analysis of primary products from *n*-hexadecane autoxidation at 120-180.degree.C. *J Am Chem Soc* 101:7574–7584.
8. Jalan A, et al. (2013) New pathways for formation of acids and carbonyl products in low-temperature oxidation: The Korcek decomposition of γ-ketohydroperoxides. *J Am Chem Soc* 135:11100–11114.
9. Davis AC, Francisco JS (2011) Reactivity trends within alkoxy radical reactions responsible for chain branching. *J Am Chem Soc* 133:18208–18219.
10. Ehn M, et al. (2014) A large source of low-volatility secondary organic aerosol. *Nature* 506:476–479.
11. Jokinen T, et al. (2015) Production of extremely low volatile organic compounds from biogenic emissions: Measured yields and atmospheric implications. *Proc Natl Acad Sci USA* 112:7123–7128.
12. Pollard RT (1977) Hydrocarbons. *Comprehensive Chemical Kinetics: Gas-Phase Combustion*, eds Bamford CH, Tipper CFH (Elsevier, Amsterdam), Vol 17, pp 249–368.
13. Griffiths JF (1969) Negative temperature-coefficient of reaction rate during hydrocarbon oxidation. *J Chem Soc D,* 483b–484.
14. Warnatz J, Maas U, Dibble RW (1999) Low temperature oxidation, engine knock. *Combustion: Physical and Chemical Fundamentals, Modeling and Simulation, Experiments, Pollutant Formation* (Springer, Berlin), pp 227–236.
15. Zádor J, Taatjes CA, Fernandes RX (2011) Kinetics of elementary reactions in low-temperature autoignition chemistry. *Pror Energy Combust Sci* 37:371–421.
16. Wang Z, et al. (2016) Additional chain-branching pathways in the low-temperature oxidation of branched alkanes. *Combust Flame* 164:386–396.
17. Wang Z, et al. (2017) New insights into the low-temperature oxidation of 2-methylhexane. *Proc Combust Inst* 36:373–382.
18. Rissanen MP, et al. (2014) The formation of highly oxidized multifunctional products in the ozonolysis of cyclohexene. *J Am Chem Soc* 136:15596–15606.
19. Berndt T, et al. (2016) Hydroxyl radical-induced formation of highly oxidized organic compounds. *Nat Commun* 7:13677.
20. D'Ambro EL, et al. (2017) Isomerization of second-generation isoprene peroxy radicals: Epoxide formation and implications for secondary organic aerosol yields. *Environ Sci Technol* 51:4978–4987.
21. Riccobono F, et al. (2014) Oxidation products of biogenic emissions contribute to nucleation of atmospheric particles. *Science* 344:717–721.
22. Jokinen T, et al. (2014) Rapid autoxidation forms highly oxidized RO_2 radicals in the atmosphere. *Angew Chem Int Ed Engl* 53:14596–14600.
23. Crounse JD, Nielsen LB, Jørgensen S, Kjaergaard HG, Wennberg PO (2013) Autoxidation of organic compounds in the atmosphere. *J Phys Chem Lett* 4:3513–3520.
24. Qi F (2013) Combustion chemistry probed by synchrotron VUV photoionization mass spectrometry. *Proc Combust Inst* 34:33–63.
25. Kohse-Höinghaus K, et al. (2010) Biofuel combustion chemistry: From ethanol to biodiesel. *Angew Chem Int Ed Engl* 49:3572–3597.
26. Moshammer K, et al. (2015) Detection and identification of the keto-hydroperoxide ($HOOCH_2OCHO$) and other intermediates during low-temperature oxidation of dimethyl ether. *J Phys Chem A* 119:7361–7374.
27. Moshammer K, et al. (2016) Quantification of the keto-hydroperoxide ($HOOCH_2OCHO$) and other elusive intermediates during low-temperature oxidation of dimethyl ether. *J Phys Chem A* 120:7890–7901.
28. Raffaelli A, Saba A (2003) Atmospheric pressure photoionization mass spectrometry. *Mass Spectrom Rev* 22:318–331.
29. Hu Q, et al. (2005) The orbitrap: A new mass spectrometer. *J Mass Spectrom* 40: 430–443.
30. Wang Z, et al. (2018) n-Heptane cool flame chemistry: Unraveling intermediate species measured in a stirred reactor and motored engine. *Combust Flame* 187:199–216.
31. Fenter FF, Catoire V, Lesclaux R, Lightfoot PD (1993) The ethylperoxy radical: Its ultraviolet spectrum, self-reaction, and reaction with hydroperoxy, each studied as a function of temperature. *J Phys Chem* 97:3530–3538.
32. Sharma S, Raman S, Green WH (2010) Intramolecular hydrogen migration in alkylperoxy and hydroperoxyalkylperoxy radicals: Accurate treatment of hindered rotors. *J Phys Chem A* 114:5689–5701.
33. Battin-Leclerc F, et al. (2010) Experimental confirmation of the low-temperature oxidation scheme of alkanes. *Angew Chem Int Ed Engl* 49:3169–3172.
34. Hansen N, Cool TA, Westmoreland PR, Kohse-Höinghaus K (2009) Recent contributions of flame-sampling molecular-beam mass spectrometry to a fundamental understanding of combustion chemistry. *Pror Energy Combust Sci* 35:168–191.
35. Pelucchi M, et al. (2014) Improved kinetic model of the low-temperature oxidation of *n*-heptane. *Energy Fuels* 28:7178–7193.
36. Savee JD, et al. (2015) Carbon radicals. Direct observation and kinetics of a hydroperoxyalkyl radical (QOOH). *Science* 347:643–646.
37. Rodriguez A, et al. (2017) Measuring hydroperoxide chain-branching agents during *n*-pentane low-temperature oxidation. *Proc Combust Inst* 36:333–342.
38. Battin-Leclerc F, et al. (2011) New experimental evidences about the formation and consumption of ketohydroperoxides. *Proc Combust Inst* 33:325–331.
39. Zheng J, Truhlar DG (2013) Quantum thermochemistry: Multistructural method with torsional anharmonicity based on a coupled torsional potential. *J Chem Theory Comput* 9:1356–1367.
40. Bao JL, Meana-Paneda R, Truhlar DG (2015) Multi-path variational transition state theory for chiral molecules: The site-dependent kinetics for abstraction of hydrogen from 2-butanol by hydroperoxyl radical, analysis of hydrogen bonding in the transition state, and dramatic temperature dependence of the activation energy. *Chem Sci (Camb)* 6:5866–5881.
41. Xing L, Zhang L, Zhang F, Jiang J (2017) Theoretical kinetic studies for low temperature oxidation of two typical methylcyclohexyl radicals. *Combust Flame* 182: 216–224.
42. Ning H, Gong C, Tan N, Li Z, Li X (2015) Low- and intermediate- temperature oxidation of ethylcyclohexane: A theoretical study. *Combust Flame* 162:4167–4182.
43. Wang Z, Sarathy MS (2016) Third O_2 addition reactions promote the low temperature ignition of *n*-alkanes. *Combust Flame* 165:364–372.
44. Pei Y, Hawkes ER, Kook S, Goldin GM, Lu T (2015) Modelling *n*-dodecane spray and combustion with the transported probability density function method. *Combust Flame* 162:2006–2019.
45. Cuoci A, et al. (2017) Flame extinction and low-temperature combustion of isolated fuel droplets of *n*-alkanes. *Proc Combust Inst* 36:2531–2539.